Heat Transport by Mesoscale Eddies in an Ocean Circulation Model

SYBREN S. DRIJFHOUT

Royal Netherlands Meteorological Institute, De Bilt, the Netherlands

(Manuscript received 3 August 1992, in final form 26 May 1993)

ABSTRACT

The role of mesoscale eddies in the poleward heat transport in the ocean is investigated; in particular, the compensation of poleward eddy heat transport by an eddy-induced mean meridional circulation is examined.

A multilayer isopycnic primitive equation model of an idealized western North Atlantic is presented to test whether compensation also occurs within an isopycnic model and when the poleward eddy heat transport becomes comparable to the mean transport.

Also, in this model configuration compensation of the poleward eddy heat transport arises. It is brought about by a westward eddy heat transport in the midlatitude jet, which results in a pressure drop across the basin and consequently in a modified mean meridional overturning.

This compensation is discussed within the framework of wave–mean flow interaction. It is demonstrated that compensation results from eddy–mean flow interaction when the diabatic forcing is sufficiently weak; rings are recaptured before their SST anomaly is modified significantly. When the time scale of SST anomalies is smaller than the lifetime of mesoscale rings, it is hypothesized that the non–heat transport character of eddies breaks down.

1. Introduction

Mesoscale eddies in the ocean are the dynamical analogs of atmospheric cyclones and anticyclones. It is well established that the latter play a fundamental role in the maintenance of the general circulation of the atmosphere by the transport of heat and momentum (e.g., Palmen and Newton 1969).

The role of mesoscale eddies in the ocean circulation is less well understood. This is partly due to their much smaller horizontal scale, which makes a considerably larger observational dataset necessary in order to assess their role in the maintenance of the general circulation as compared to the atmosphere. In contrast to this demand, there is at present no synoptic three-dimensional network for observations in the ocean.

One way to cope with the problem of a lack of observational data is by studying eddy–mean flow interactions in eddy-resolving, basin-scale numerical models. Such studies have been initiated after the discovery that mesoscale fluctuations often dominate the flow field in the ocean. The pioneering work on this problem has been summarized in Robinson (1983).

Recent work strongly focuses on the role of eddies in mixing and homogenization of potential vorticity (e.g., Rhines and Young 1982; Holland et al. 1984; Cox 1985; Böning and Cox 1988). Cox (1985) was the first to explicitly compare the heat budget between an eddy-resolving and a non-eddy-resolving model version. Both this study and a later one by Böning and Budich (1992) show that the air–sea heat exchange within an ocean model is insensitive to changes in horizontal resolution and diffusion, even when these changes allow the spontaneous development of mesoscale eddies by baroclinic and barotropic instability.

This result is nontrivial as those models use restoring boundary conditions with respect to temperature; that is, the vertical heat flux at the interface is determined by relaxing the sea surface temperature to a prescribed value. The eddy field causes significant changes in the dynamics of the flow, the momentum, and energy and vorticity budgets, while the heat budget remains almost unaffected. The poleward eddy heat transport appears to be compensated by an eddy-induced change of the heat transport by the mean flow.

The question arises whether this result is restricted to specific models and/or flow fields, or whether this is a general feature of ocean eddies. It remains to be clarified how and why compensation of the poleward eddy heat transport occurs; that is, why are the zonally averaged meridional temperature gradient and the air–sea heat exchange unaffected by ocean eddies?

In a series of papers, K. Bryan (1986, 1987, 1991) addresses these questions, focusing on the meridional overturning. He points out that the zonally averaged mass transport can be separated into different cells (Fig. 1). The main cell is the model counterpart of the large-scale thermohaline circulation with deep convection

Corresponding author address: Dr. Sybren S. Drijfhout, Royal Netherlands Meteorological Institute, P.O. Box 201, 3730 AE De Bilt, the Netherlands.

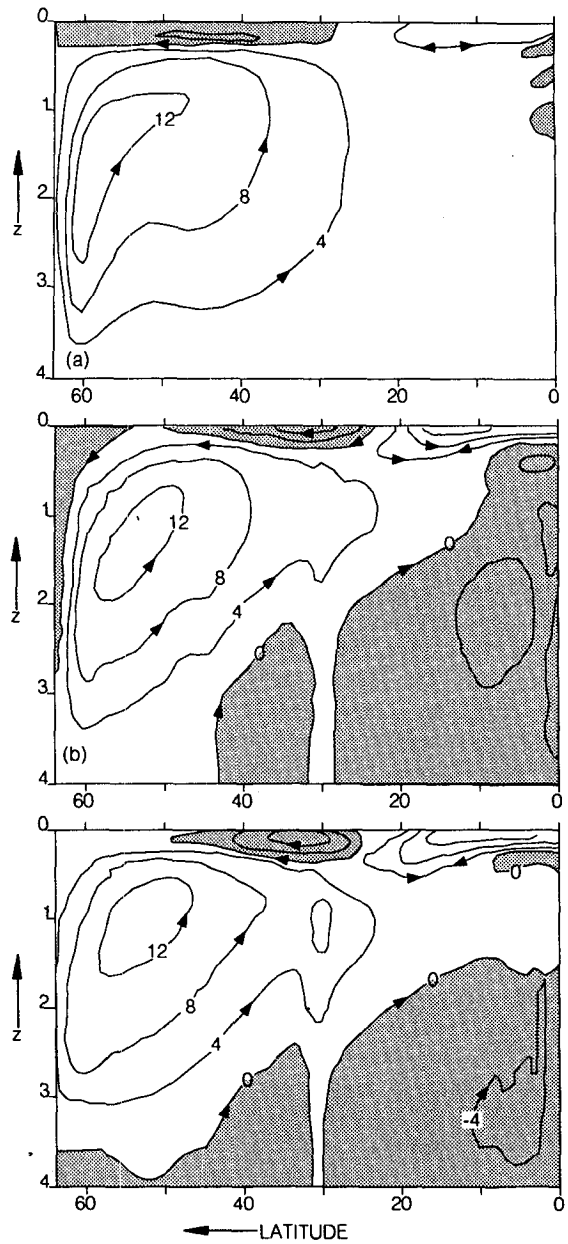

FIG. 1. The transport streamfunction of the total, zonally integrated meridional circulation in units of megatons s^{-1}. (a) The low resolution, non-eddy-resolving case of Cox (1985), (b) the intermediate resolution case of Cox (1985), and (c) the highest resolution case of Böning and Budich (1992).

in the northern part and diffusive upwelling in the rest of the basin. The two smaller cells that are confined to the surface layers are the effect on the meridional mass transport of wind forcing in the presence of a thermohaline forcing.

These overturning cells cannot simply be derived a priori, as they result from a nonlinear balance: they form a combination of the zonally averaged Ekman, Sverdrup, and boundary current transports modified by buoyancy forcing. Both the location and the strength of the overturning cells depend on the resolution and friction parameterization (Fig. 1). Their latitudinal scale is about the scale of the wind field. Henceforth, we shall name them wind-scale overturning cells.

In the subtropical region the wind-induced overturning is clockwise, resulting in a northward heat transport; in the midlatitudes the reverse situation occurs. Baroclinic instability counteracts the effect of the wind-scale overturning cells. The eddies transport heat southward in the subtropics and northward in the midlatitudes.

If in a numerical model the baroclinic instability is increased by an enhancement of the resolution and a decrease of the friction, the mean flow shows an increase of the wind-scale overturning cells, adding to the compensation of the poleward eddy heat transport.

This study investigates the validity of the mechanism sketched above. Three goals have been pursued: the first one is to test the robustness of the compensation of the eddy heat transport by the mean flow with respect to model formulation and flow field. The second goal is to investigate how this compensation occurs, that is, what causes the enhancement of the wind-scale overturning cells that counteract the poleward eddy heat transport. The third goal is to examine the possible reason why the poleward eddy heat transport and the eddy-induced heat transport by the wind-scale overturning cells not only counteract but also almost balance.

The outline of the paper is as follows. A description of the numerical model is given in section 2. A comparison of the coarse- and fine-grid solutions is given in section 3. In section 4 the eddy–mean flow interaction that causes the eddy-induced enhancement of the wind-scale overturning cells is analyzed. In section 5 we discuss the compensation of the poleward eddy heat transport and the role of the diabatic forcing. In section 6 we summarize and present our conclusions.

2. Description of the numerical model

A three-layer primitive equation isopycnic model is used following the principles outlined by Bleck and Boudra (1986). The use of such a model was suggested by Drijfhout (1992) for the following reason: In Cartesian primitive equation (PE) models an enhancement of the resolution can result in a decrease of the spurious diapycnal mixing of heat. As nonlinear processes can amplify this spurious effect by orders of magnitude, the decreased spurious mixing could possibly balance an enhanced eddy heat transport.

The usual simplifications, in the form of the hydrostatic, the Boussinesq, and the β-plane approximation and the incompressibility condition have been applied. Instead of Laplacian friction, the more scale selective biharmonic friction is used (see Holland 1978).

Model domain and wind forcing are the same as in Semtner and Mintz (1977) (Fig. 2). Relative to this

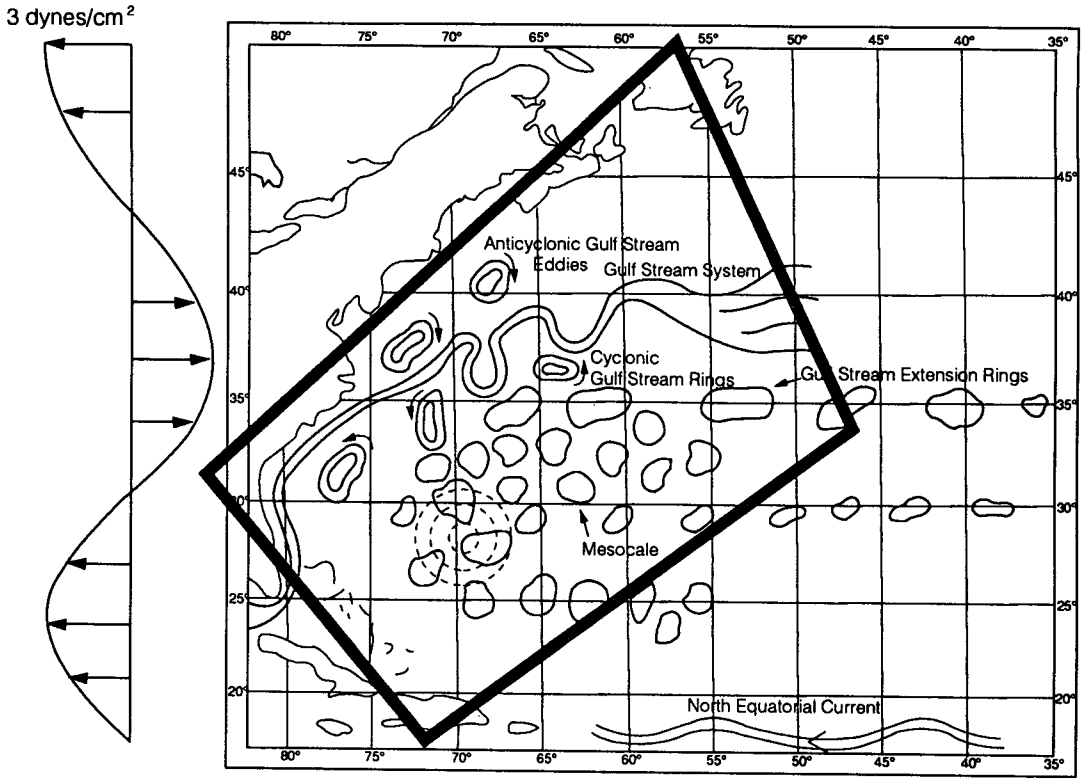

FIG. 2. The boundary of the model domain, superimposed on a schematic picture of mesoscale variability in the western portion of the North Atlantic. Also shown is the zonal wind stress that drives the model ocean. The upper-layer depth is relaxed to prescribed values that show a linear variation with latitude. Extreme values are −260 m at the northern tip and 660 m at the southern tip of the domain.

model, a few simplifications have been made justified by the model comparison and parameter study in Semtner and Holland (1978). As the model domain is rather small the spherical dependence of the coordinates is dropped. Also, the vertical resolution is reduced to three layers, with the interfaces at an average depth of 200 m and 600 m. The reduced gravities at the interfaces are, respectively, $g'_1 = 1.3 \times 10^{-2}$ m s^{-2}, and $g'_2 = 0.7 \times 10^{-2}$ m s^{-2}, corresponding to a temperature difference between layers 1 and 2 of 6.5°C, and 3.5°C for layers 2 and 3.

The momentum equations of the model are

$$u_t + (\mathbf{u}^2/2)_x - (f+\zeta)v = -M_x - B_M\nabla^4 u + \frac{1}{\Delta h}(g\Delta\tau_x), \quad (2.1)$$

$$v_t + (\mathbf{u}^2/2)_y + (f+\zeta)u = -M_y - B_M\nabla^4 v + \frac{1}{\Delta h}(g\Delta\tau_y). \quad (2.2)$$

In these equations $\mathbf{u} = (u, v)$ is the horizontal velocity, f is the Coriolis parameter, $\zeta = v_x - u_y$ is the relative vorticity, $M = gz + p/\rho$ is the Montgomery potential, g is the gravity acceleration, p represents the pressure, Δh is the thickness of the isopycnic layer, $(\Delta\tau_x, \Delta\tau_y)$ are the wind and bottom drag-related stress differences in the x and y direction between the top and bottom of a coordinate layer. Equations (2.1) and (2.2) apply to all three layers, although in most parts of the second layer $\Delta\tau x$ and $\Delta\tau y$ will be zero: The wind stress is assumed to decrease linearly within a layer of 100 m. If the surface layer(s) is (are) shallower than this value, part of the wind stress is passed to the layer below. A quadratic bottom stress is used. We assume that it decreases linearly within a layer of 10 m. If the third layer becomes shallower than this value the second layer starts feeling the bottom.

In (2.1) and (2.2) B_M is a viscosity parameter. (In some experiments the biharmonic friction is replaced by Laplacian friction: $A_M\nabla^2 u$.) The lateral boundary condition for the velocity is a free-slip condition.

The hydrostatic equation reads

$$M_s = p\frac{\partial}{\partial s}(1/\rho), \quad (2.3)$$

where s is the vertical coordinate of the isopycnic model.

The equation for the layer thickness h reads

$$\frac{\partial}{\partial t} h + \nabla \cdot \mathbf{U} = -B_T \nabla^4 h + \gamma(h^* - h), \quad (2.4)$$

where $\mathbf{U}$ is the horizontal mass transport. (In some experiments $B_T \nabla^4 h$ has been replaced by a Laplacian friction: $A_T \nabla^2 h$.) The lateral boundary condition for the layer thickness is a no-flux condition. For the numerical formulation of the boundary conditions, we refer to Semtner and Mintz (1977).

Equation (2.4) is different from the continuity equation in Bleck and Boudra (1986) by the appearance of the right-hand-side terms. We have chosen to use an isopycnal diffusion of layer thickness (apparent temperature) to keep the model as close as possible to the formulation of the Semtner and Mintz (1977) and Cox and Bryan (1984) models. Moreover, Bleck and Boudra use a different formulation for the viscosity, making it dependent on the layer thickness. To test whether this choice of friction parameterization seriously influences the model results, we have tested the different types of friction and diffusion formulations and found no significant differences in the model results.

Another difference from the Bleck and Boudra model is the buoyancy forcing term $\gamma(h^* - h)$. In the isopycnic model an upper-layer thickness anomaly Δh corresponds to a heat anomaly $\Delta h(\bar{T}_1 - \bar{T}_2)$, where the latter term denotes the (basin averaged) temperature difference between the first and second layer. In a Cartesian model, a temperature anomaly ΔT corresponds to a heat anomaly $\Delta T \Delta z$, where the latter term denotes the layer depth. In the isopycnic model, the heat content of the upper layer is zero when h is zero; in the Cartesian model, this is zero when T equals $\bar{T}_2$. For the upper layer, an apparent temperature T related to the layer thickness h can be defined by equating the two definitions of heat in the isopycnic, respectively, Cartesian framework:

$$(T - \bar{T}_2)\Delta z = h(\bar{T}_1 - \bar{T}_2). \quad (2.5)$$

With this formula the Haney forcing (Haney 1971), $\partial T/\partial t = \gamma(T^* - T)$, can be rewritten as $\partial h/\partial t = \gamma(h^* - h)$.

The coefficient γ times Δz (or $\gamma \bar{h}$) is 0.6 m day^{-1}; the same value as in Semtner and Mintz (1977). With an average upper-layer depth of 200 m this is equivalent to a relaxation time for surface thickness (temperature) anomalies of 333 days. Here h^* is related to the atmospheric forcing temperature T^* by

$$h^* - \bar{h} = \frac{(T^* - \bar{T}_1)\Delta z}{(\bar{T}_1 - \bar{T}_2)}. \quad (2.6)$$

With an average layer depth of 200 m and a temperature difference between the first and second layer of 6.5°C, a north–south variation in h^* of 920 m is equivalent to a north–south variation in T^* of 30°C (prescribed in Semtner and Mintz 1977). This means that h^* varies linearly with latitude from −260 m at the northern boundary of the basin to +660 m at the southern boundary. Negative values for h^* can be understood as the analog of relaxing temperatures at the upper level to a temperature below the average temperature at the second level in a Cartesian model.

The equation for layer thickness, Eq. (2.4), is solved with a flux-corrected transport (FCT) algorithm (Bleck and Boudra 1986). The FCT algorithm prevents the overshoot caused by the normally used second-order schemes and avoids the occurrence of layers with negative thickness.

Whenever the surface heat flux creates a negative thickness, the heat flux is reduced until the layer thickness becomes zero. With this correction the basin-averaged surface heat flux is no longer zero. We have chosen to prohibit the resulting "climate drift" in the model by redistributing the heat flux residue at all nonzero mass gridboxes of the upper layer. (Within the present model relaxing this constraint did not yield significantly different results.)

Also when outcropping occurs, buoyancy forcing is not applied to the second layer. If we would do so, the resulting loss of mass from the second layer must be balanced by a diapycnal diffusivity; forcing upwelling from the bottom layer to the middle layer. This would introduce extra physical processes, with very long time scales. As this study focuses on the modification of the wind-scale overturning cells by the eddies and the subsequent eddy-induced change in heat transport by the mean flow, the exclusion of deep convection as a mode of heat transport is not relevant for this process study. [For a review of the relation between vertical diffusion, deep convection, and heat transport we refer to F. Bryan (1987).]

Bottom topography is the same as in Semtner and Mintz (Fig. 3). The intersection of isopycnals with the bottom can cause large technical difficulties (e.g., Bleck and Smith 1990). These problems have been circumvented by using a (variable) land–sea mask for all the isopycnic layers. The use of bottom topography introduces weighting factors in the formulation of thickness dissipation. This is to ensure that no spurious barotropic mass flux arises from one column of grid boxes to another.

3. Comparison of solutions

a. Flow fields and energetics

We initialize with zero velocities and zero thickness gradients everywhere. Figure 4 shows the time evolution of the basin-averaged kinetic energy. The first 30 years have been run with a coarse-grid configuration; a horizontal resolution of 74 km (about $2/3° \times 2/3°$). Laplacian friction has been used, the viscosity parameter A_M is 10^3 m^2 s^{-1}, and the diffusivity parameter A_T is 0.5×10^3 m^2 s^{-1}. The viscosity parameter is chosen equal as in Semtner and Mintz (1977), the diffu-

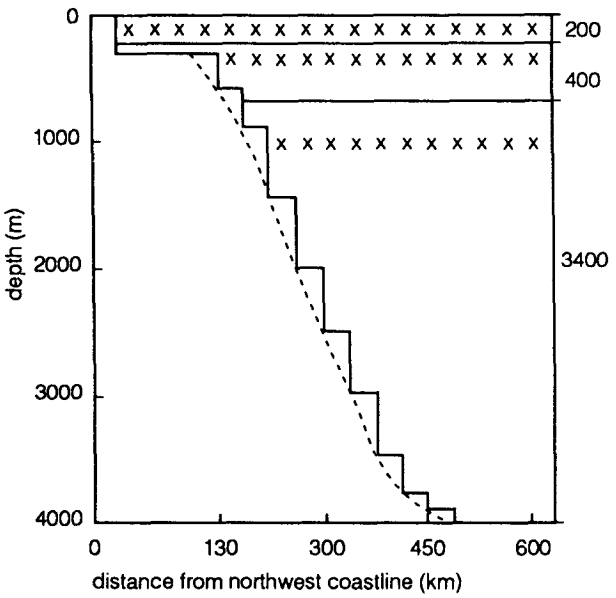

FIG. 3. Model topography and grid box placement near the northwest coastline, for the model version of 1/3° × 1/3° resolution.

sivity parameter half their value. The reason for this choice is that the isopycnic model responds differently to the friction parameterization compared to the Cartesian primitive equation model. With the present friction parameterization the higher diffusivity parameter suppresses the transients stronger than within a Cartesian model.

At year 30 the grid size is decreased to 37 km. The model responds with higher kinetic energies (Fig. 4), although the friction is unchanged.

At year 40 the friction parameters have been decreased: A_M is 0.2×10^3 m^2 s^{-1} and A_T is 0.3×10^3 m^2 s^{-1}. Now the flow becomes unsteady; a weak eddy field appears, which causes transient behavior. The energy shows a small amplitude modulation on the time-averaged value.

At year 50 we have changed from Laplacian friction to biharmonic friction. Now the viscosity parameter B_M is 0.8×10^{11} m^4 s^{-1}, and the diffusivity parameter B_T is 1.2×10^{11} m^4 s^{-1}. With this type of friction parameterization, the wind input is no longer balanced by the lateral viscosity (e.g., Holland 1978). The flow field responds with increased momentum and kinetic energy until it becomes baroclinically unstable. Eddies induce an enhancement of the downward transport of momentum. Now the wind input is mainly balanced by bottom friction. Modulations in kinetic energy level have increased, with dominant frequencies O[(50–100 days)$^{-1}$], related to instability processes. There are also vacillations with longer time scales O (3 years). Such vacillations are analyzed in Cox (1987). Because of these vacillations one has to take averages of eddy and mean flow statistics over a period of at least three to four years.

At year 60 we have decreased both the horizontal resolution to 18.5 km and the friction parameters. Now B_M is 0.3×10^{10} m^4 s^{-1}, and B_T is 0.45×10^{10} m^4 s^{-1}. This again results in an enhancement of the kinetic energy; the downward transport of momentum through the baroclinic instability mechanism becomes more efficient, and a larger part of the wind input is balanced by bottom friction. The importance of lateral friction has been reduced further. This results in larger amplitudes for the higher frequencies up to (100 days)$^{-1}$. Although there are some quantitative differences between the average statistical equilibrium at year 65 and year 60, there are no qualitative differences between the two equilibria with 18.5-km and 37-km resolution, both using biharmonic friction. The forcing has been chosen such that the model exhibits more baroclinic instability than the models of Cox (1985) and Böning and Budich (1992). Therefore, the energy spectrum already peaks at the mesoscale in the run with 37-km resolution and biharmonic friction. Reducing the resolution and friction further will not qualitatively alter this picture.

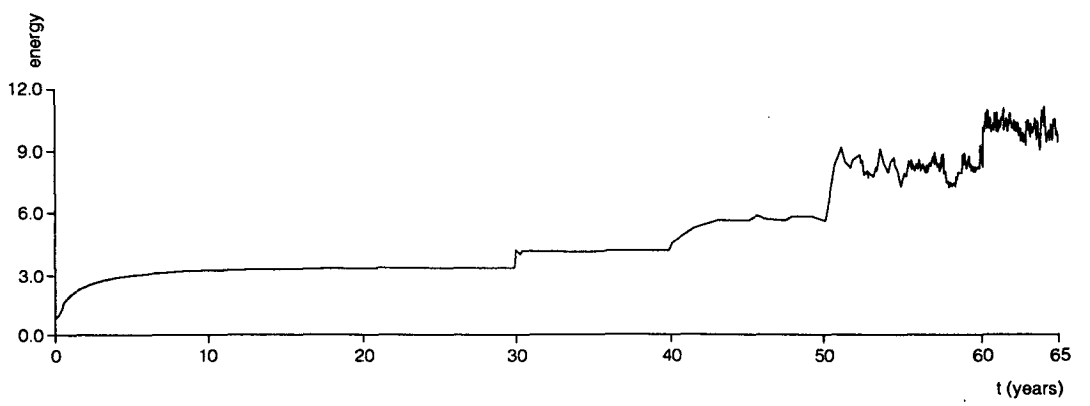

FIG. 4. Basin-averaged kinetic energy in 10^{-3} m^2 s^{-2} as a function of time.

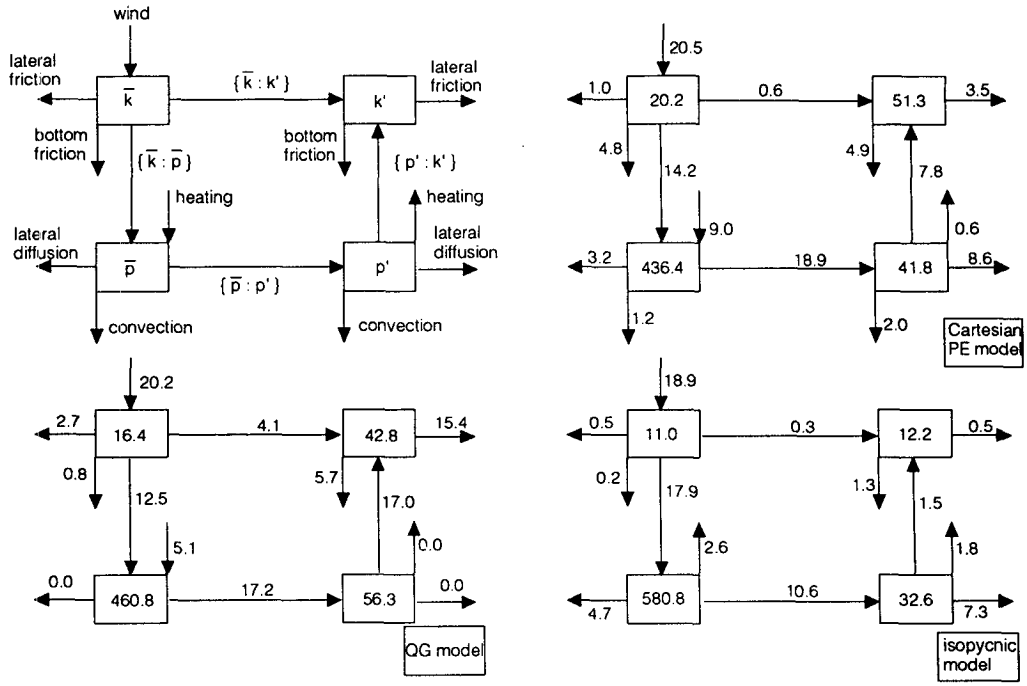

FIG. 5. Basin-averaged energetics of the isopycnic model versus the Cartesian PE and quasigeostrophic experiments of Semtner and Holland (1978). Energies are in kJ m^{-2} and rates are in kJ m^{-2} $(10^6 s)^{-1}$.

From now on the run between year 30 and 40 will be called experiment 1, the run from year 60 to 65 will be called experiment 2.

Figure 5 shows the basin-averaged energy budget for experiment 2, compared to the budgets for the Cartesian PE model and the quasigeostrophic model of this domain (see also Semtner and Holland 1978). The basin-averaged mean and eddy kinetic energy and the eddy potential energy are substantially smaller within the isopycnic model. In all three models, about an equal amount of mean kinetic energy is produced by the wind stress; also an equal amount of mean kinetic energy is transferred to mean potential energy. However, within the isopycnic model the air–sea heat exchange destroys mean potential energy, contrary to the other two models. This must be due to the different type of buoyancy forcing. The cooling of the subtropical warm water bowl destroys more potential energy than is created by the overall increase in north–south temperature gradient. In the other two models, the latter effect dominates over the cooling of subtropical water. Also, the effect of surfacing isopycnals in the northern part of the domain, which precludes cooling the upper layer in the isopycnic model there, might contribute to this discrepancy.

The main effect of the buoyancy forcing being a sink instead of a source term for the mean available potential energy is a reduction in conversion to eddy potential and kinetic energy compared to Cartesian coordinate models. However, upper-layer values of eddy kinetic energy (Fig. 6) still are on the order of 70% of the values in the Cartesian PE model, while the upper layer in the isopycnic model is twice as thick. It is mainly through a relative absence of eddies and mean flow in the deep layer, that the eddy energies and mean kinetic energy are much lower in the isopycnic model compared to the other models. Relative to the Cartesian models the barotropic mode is suppressed, but the baroclinic mode is almost unaffected. As the heat transport is determined by the baroclinic mode, we assume that the relative lack of a barotropic mode does not substantially affect the processes that are the subject of this study.

The time-averaged barotropic streamfunction and upper-layer thickness for experiments 1 and 2 show a two and a half gyre pattern that is consistent with the wind forcing (Fig. 7a). A model counterpart of the separated Gulf Stream is evident at the boundary of the subtropical and subpolar gyre. The mass transport is enhanced in experiment 2 due to the downward transport of momentum by the eddies. However, the inertial circulation is only slightly enhanced by the strong eddy activity, compared to the Cartesian primitive equation and quasigeostrophic simulations of Semtner and Holland (1978). The most obvious qualitative difference between the average mass transport fields is a standing wave pattern at the gyre boundary in experiment 2. The overall structure shows much more small-scale detail.

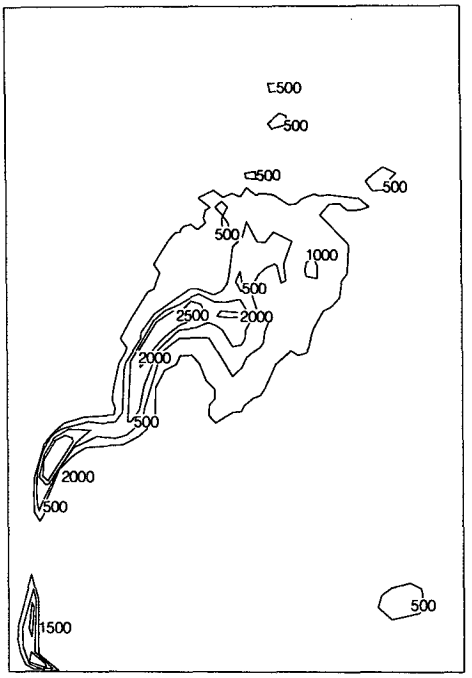

FIG. 6. Distribution of eddy kinetic energy (in $cm^2\ s^{-2}$) for the upper layer. (The north is veered 45° backward.)

The same holds for the time-averaged upper-layer thickness (Fig. 7b). In both experiments outcropping in the northern part is limited to the interior of the subpolar gyre. The subtropical gyre is clearly visible in the upper-layer thickness fields, demonstrating the dominance of wind forcing over buoyancy forcing in this calculation. Huang (1989) defines a nondimensional parameter $\Gamma = 2\beta L^2\gamma\Delta p/\tau$ to measure the relative strength of buoyancy forcing to wind forcing. (L is the latitudinal scale of the wind forcing.) This parameter measures the ratio of the circulation time of the wind-driven gyres to the relaxation time of the upper-layer temperature field to the buoyancy forcing. In the present study Γ varies from values of 0.0 within the subpolar gyre to 1.0 within the subtropical gyre. The average value is 0.4, the same as in Semtner and Mintz. Clearly, both in this experiment and in the experiment of Semtner and Mintz (1977) the thermal forcing is relatively weak, due to the small size of the basin which makes the circulation time of the wind-driven gyres short.

The instantaneous upper-layer thickness fields show a highly turbulent flow, with a much narrower and intense Gulf Stream, strongly meandering (Fig. 8). The basin is filled with numerous eddies. The formation of a cold core ring can easily be followed in this sequence. The smoothness of the time-averaged fields of experiment 2 compared to the instantaneous fields must be attributed to the variability of the sharper frontal structures. The eddies smear out gradients in a time-averaged sense. Both the time-averaged and instantaneous fields show qualitative agreement with the Cartesian PE model simulations of Semtner and Mintz (1977) and the quasigeostrophic simulations of Semtner and Holland (1978).

b. Meridional heat transport

The meridional (poleward) heat transport can be evaluated by integrating the zonally and vertically integrated form of the heat budget equation (2.4a), from the southern boundary to a latitude y_0:

$$\frac{\partial}{\partial t} T + \nabla\cdot(\mathbf{u}T) = -B_T\nabla^4 T + \gamma(T^* - T). \quad (2.4a)$$

We then obtain from the thickness advection, the poleward heat transport at latitude y_0, balanced by the integral of the surface flux, diffusion, and tendency (heat storage).

Figure 9 shows this balance for experiments 1 and 2. The contribution from the (integral of the) tendency is negligible in the overall (integrated) heat budget, as it should be in statistical equilibrium. The meridional heat transport in this model is composed of the transport by the wind-scale overturning cells (northward in the subtropics and southward in midlatitudes), the northward heat transport by the subtropical and subpolar gyres, and the eddy heat transport. This results in a minimum in heat transport at the position of the central jet. (Deep convection was excluded as a mode of heat transport.)

The similarity of the integrated surface heat flux within the two model versions is striking (Fig. 9): the eddies appear not to change significantly the zonally averaged upper-layer temperature field and consequently not to change the vertical heat flux between ocean and atmosphere.

The similarity of the heat transport in our model with and without eddies is neither the result of a prescribed constant forcing nor the result of a negligible eddy heat transport. There is a large northward heat transport by the eddies at the latitude of the central jet in this model (Fig. 10). This is associated with the central jet being the primary source of baroclinic instability. But the northward eddy heat transport at the boundary between the subpolar and subtropical gyre is compensated by an increase in southward heat transport by the mean flow at this latitude.

The first question stated in the introduction has now been answered: compensation of the poleward eddy heat transport is a rather robust model feature. It also occurs within an isopycnic model, also in the case when the eddy heat transport is not a small perturbation to the total heat transport (Fig. 10). As the forcing with respect to temperature is not prescribed, there must be a dynamical imperative that prevents a change in the zonally averaged temperature and air–sea heat exchange by the eddies in this and other models (Cox 1985; Böning and Budich 1992). In the following sec-

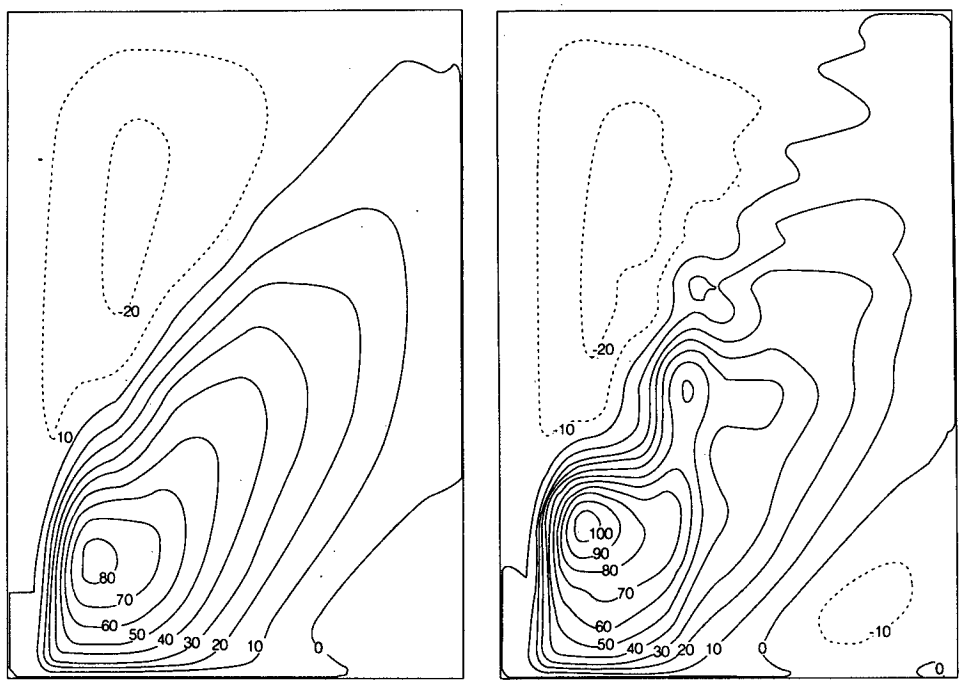

FIG. 7a. Time-averaged barotropic streamfunction for experiments 1 (left) and 2 (right). Values are in Sv $\equiv 10^6$ m^3 s^{-1}.

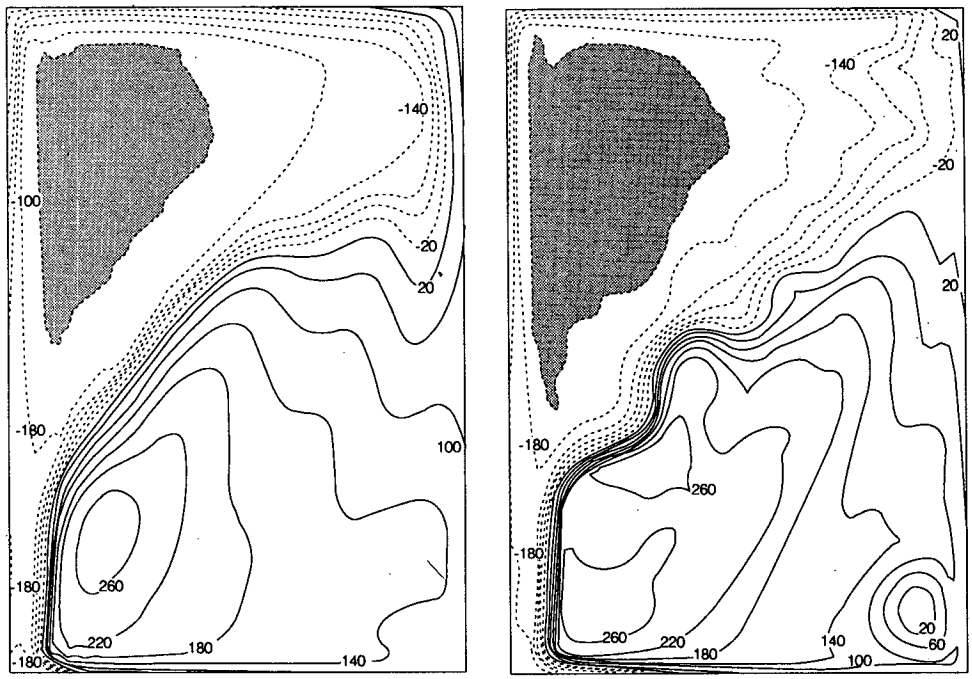

FIG. 7b. Time-averaged upper-layer thickness for experiments 1 and 2. Values are in m relative to the average thickness of 200 m. Stippled areas denote a zero thickness (outcropping).

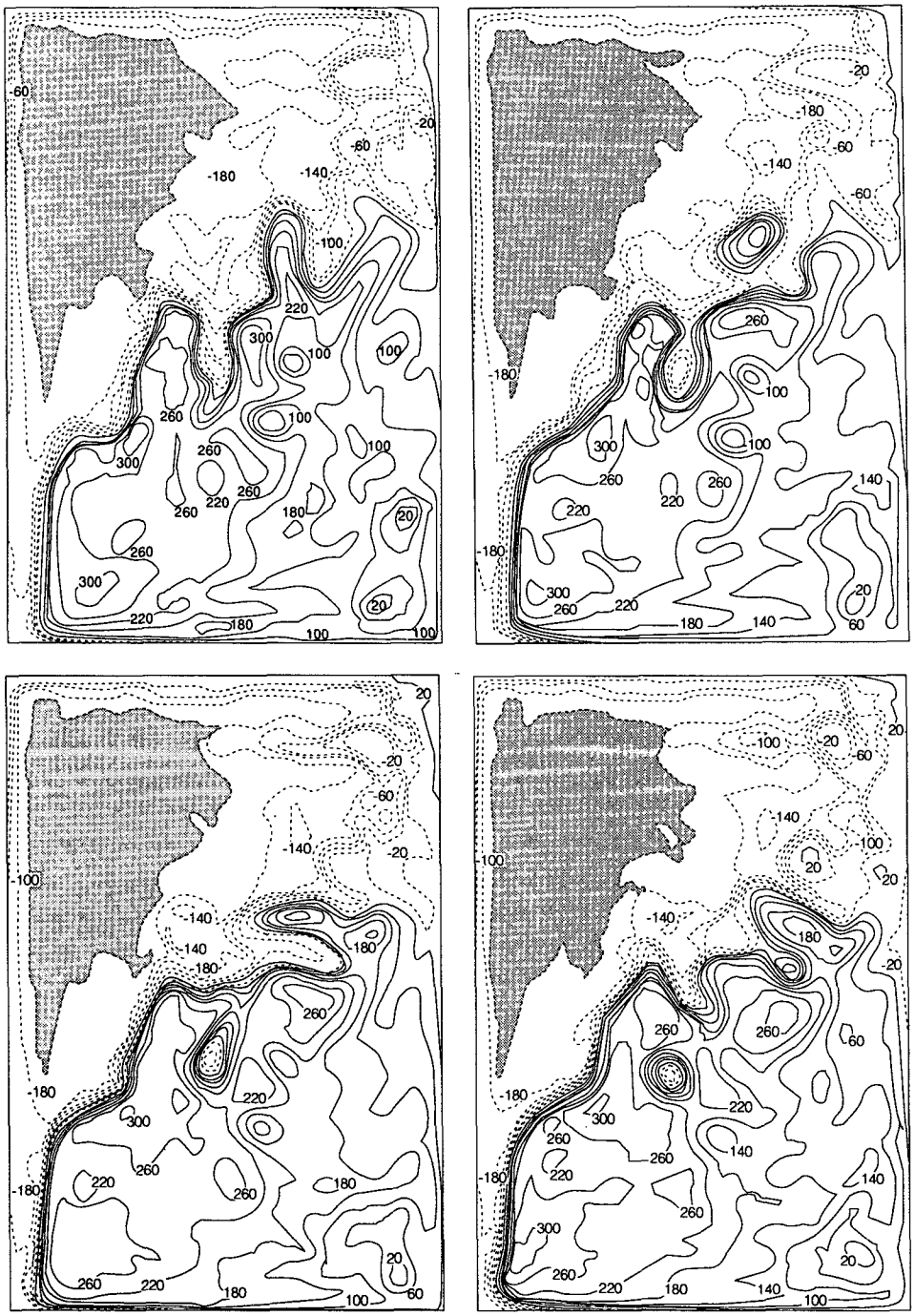

FIG. 8. Instantaneous upper-layer thickness fields for experiment 2 at 10-day intervals.

tions, an analysis is presented of how this compensation occurs.

4. Eddy–mean flow interaction

In the former section, we established the compensation of the poleward eddy heat transport in the present model. This compensation was also found by Cox (1985) and Böning and Budich (1992). Bryan (1991) suggests that the compensation in the latter two studies consists of an enhancement of the wind-scale overturning cells, which compensates the heat transport driven by baroclinic instability. Figure 11 shows that the same mechanism features in the present model: in

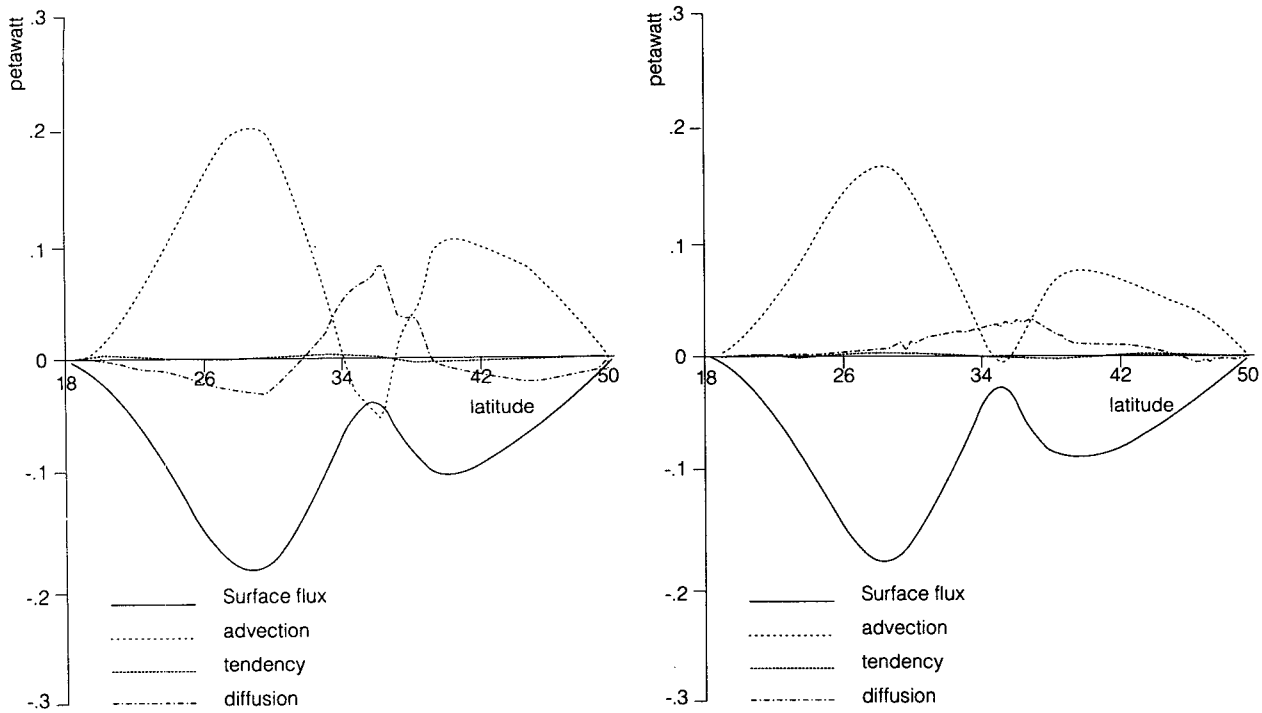

FIG. 9. Heat budget in petawatts for experiment 1 (left) and 2 (right). Shown are the integrated forms of heat advection, diffusion, surface flux, and tendency.

the eddy-resolving version of the model the transport by the anticlockwise overturning cell at midlatitudes has increased by a factor 3. The question is now, How is this accomplished in an eddy-resolving model?

Bryan (1986) pointed out that modification of the wind-scale overturning cells should be associated with a change in the cross-basin zonal pressure gradient. This would imply that the geostrophic part of the mean meridional circulation is modified and balances the poleward eddy heat transport. To test this conjecture the zonally and time-averaged zonal momentum balance for the upper layer [Eq. (2.1)] is considered. Four terms enter the first-order balance: namely, $\overline{fv}$, $\overline{M}_x$, $\overline{(g\Delta\tau_x)/(\Delta h)}$, and $\overline{\zeta v - (u^2/2)_x}$, that is, the nonlinear advection term.

Figure 12a shows the eddy-induced change in the zonal momentum balance for the first and second layer, that is, the difference between experiment 2 and 1. Terms are multiplied with the layer depth h. A difference in wind-stress results when the layer depth is more often less than 100 m, in which case part of the wind stress is passed to the second layer. It is seen that the zonal integral of the nonlinear advection terms are most important in the central section of the domain: the region of the northward flowing boundary current and the midlatitude jet. The eddy-induced change in meridional overturning cannot be completely understood without considering the eddy-induced change in the boundary currents. However, the enhancement of the anticlockwise overturning cell at midlatitudes appears to be mainly associated with an increase of the zonal pressure gradient in the upper layer and a decrease in the second layer. This is most prominently seen in Figs. 12b and 12c between 34° and 36°N. In the following we will focus on the mechanism that causes the eddy-induced change in zonal pressure gradient.

The change in zonal pressure gradient is associated with the enhancement of the meridional overturning. This change in cross-basin pressure difference is an eddy-induced baroclinic feature; the sign of this change is opposite in the first and second layer (Figs. 12b and 12c). So the change in zonal pressure gradient at midlatitudes must be associated with a change in the zonal heat distribution.

This conjecture is confirmed by Fig. 13, which shows the difference in upper-layer thickness between experiments 1 and 2. Figure 13 illustrates that the eddies have induced a change in zonal heat distribution at midlatitudes. The western side of the basin has become warmer there, the eastern side cooler. This implies a change in the zonal advection of heat. Offhand, it is not clear whether this is caused by a westward eddy heat transport or by an eddy-induced decrease in the eastward heat transport by the mean flow.

Within a zonal band the zonal heat transport cannot be calculated straightforwardly, as it would be defined for cross sections with nonzero net volume transports. However, we only want to know the qualitative effect

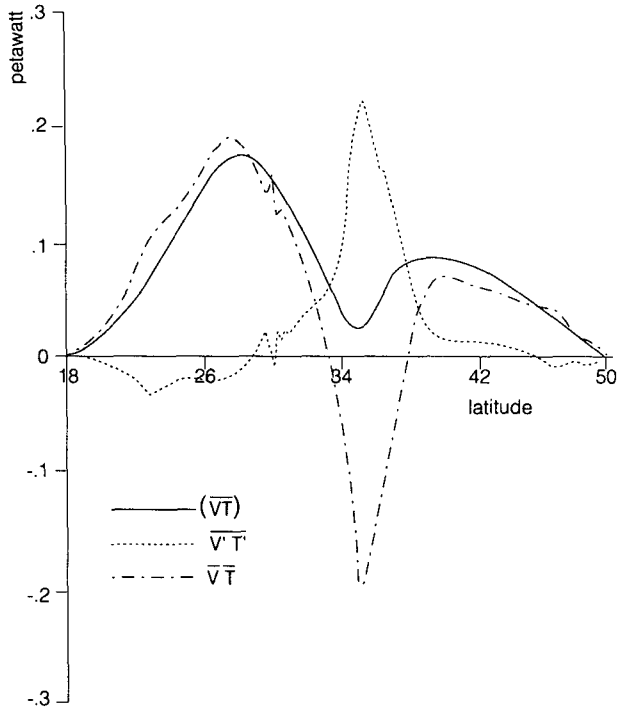

FIG. 10. Heat transport for experiment 2. Shown are the total heat transport (advection plus diffusion), the eddy heat transport, and the heat transport by the mean flow.

of the eddies on the zonal heat advection, that is, the sign of the eddy heat transport and the eddy-induced change in heat transport by the mean flow. This can be evaluated by defining heat transport relative to the lowest layer, as the overturning cells and the change in pressure gradient mainly are confined to the two upper layers.

Figure 14a compares the zonal heat transport in the latitude band depicted in Fig. 13 for experiments 1 and 2. It is seen that the total eastward heat transport by the Gulf Stream is smaller in the eddy-resolving model, consistent with the reduced temperature difference across the basin (Fig. 15). However, the heat transport by the mean flow has increased (Fig. 14b). (This is consistent with the enhancement of the mass transport by the Gulf Stream in the eddy-resolving model.) We conclude that the eddy-induced change in zonal heat transport, as defined above, is consistent with the eddy-induced change in upper-layer thickness. The negative heat transport by the eddies causes the decrease in the total zonal heat transport. The pressure change across the basin results from a westward eddy heat transport against the mean flow. For the main part this pressure change is associated with geostrophically balanced overturning anomalies that compensate the meridional eddy heat transport.

Both the westward eddy heat transport and the baroclinic energy conversion are largest where the flow turns from northward to eastward after leaving the coast (Fig. 16). Here the flow is most unstable, and the zonal temperature gradient has its maximum.

When the boundary current turns eastward and leaves the coast, the turning loop forms an anticyclonic meander to conserve its potential vorticity. This is the reason that, superposed on transient waves, a standing meander exists. The zonal scale of relative heating and cooling by the eddies, and consequently of zonal eddy heat transport and baroclinic instability, is set by the wavelength of this standing wave (cf. Figs. 6 and 16). As the amplitude of the standing wave pattern oscillates, near the western wall the large amplitude phase will induce a positive heat anomaly associated with anomalously weak zonal flow, and the weak amplitude phase induces a negative heat anomaly with anomalously strong zonal flow. This results in a negative eddy correlation of $\overline{u'T'}$.

Comparing Fig. 15 with Figs. 13 and 7b, it is seen that for experiment 2 the relatively small upper-layer depth at the eastern boundary is associated with the cold slope water: the sharp increase at 75°W with the turning of the midlatitude jet to an eastward direction and the minimum at 71°W with the southward meander that introduces extra cold water. It follows that the westward zonal eddy heat transport is downgradient at the location where the Gulf Stream turns from a northward to an approximate eastward direction. This was also found in observations by Dewar and Bane (1989). There is no clear support from observations whether a westward eddy heat transport exists within the eastward flowing Gulf Stream.

We conclude this section by noting that it has been clarified how the eddies cause pressure changes across the basin and induce mean flow changes that counteract the effect of the meridional eddy heat transport on the zonally mean meridional temperature gradient: The baroclinic instability induces a downgradient eddy heat transport in both meridional and zonal directions. The resulting decrease of zonal temperature gradient is associated with a decrease of the zonally averaged geostrophic meridional flow. This results in an enhancement of the meridional overturning, counteracting the meridional eddy heat transport. Why these effects nearly balance is not yet clear. This will be discussed further in the next section.

5. The role of diabatic forcing

The near compensation in poleward heat transport between eddies and an eddy-induced change in the mean circulation was first discussed by Bryan (1986). He presented a tentative mechanism for the compensation of eddy transports. This issue has been elaborated further in Bryan (1991). He points to similarities with the dynamics of transients in the stratosphere (reviewed by Andrews et al. 1987). The non–heat transport behavior by ocean eddies might be understood if a non-acceleration theorem can be applied (Andrews and

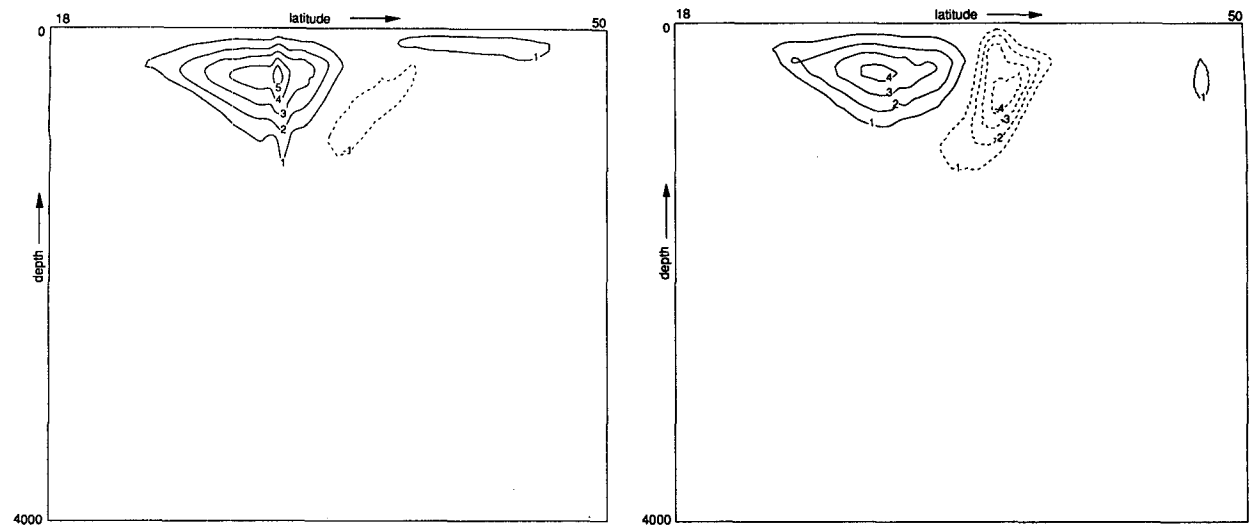

FIG. 11. Meridional transport function (Sv) for experiments 1 (left) and 2 (right).

McIntyre 1976), that is, if the waves are steady and conservative.

However, to apply a nonacceleration theorem to the transient eddies implies the development of an equivalent of the Eliassen–Palm concept (Eliassen and Palm 1961) in time-averaged conditions. This is far from trivial (e.g., Hoskins et al. 1983; Plumb 1986; Andrews 1990). Moreover, wind and buoyancy forcing in the ocean and the presence of zonal barriers would complicate significantly such a theory. In this section some of the results of the Eliassen–Palm theory will be used to comment on the role of diabatic forcing in the non-heat transport behavior of transient eddies in the model at hand. An exhaustive explanation of the interaction between transient eddies and the time-averaged flow in the ocean with the use of an equivalent Eliassen–Palm theory, however, is beyond the scope of this paper.

As a starting point, some of the results of Andrews (1983) are used. This paper treats the generalized Eliassen–Palm concept in isopycnic coordinates. If $\bar{x}$ is defined as the zonal average of x, the quasigeostrophic approximation of the mean equation for the zonal mass flux becomes

$$\bar{U}_t = f\bar{V} + \Lambda - \bar{h}\bar{M}_x + \bar{X}, \qquad (5.1)$$

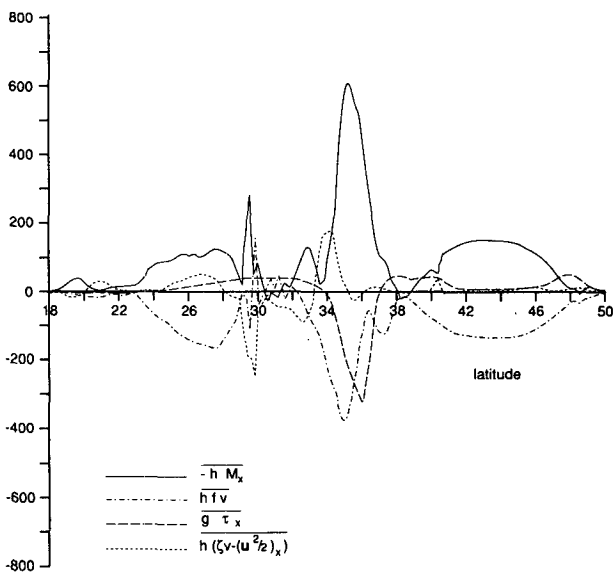

FIG. 12a. The eddy-induced change in the zonally integrated upper-layer zonal momentum balance (in $m^3 s^{-2}$). (Terms are multiplied with the layer depth.)

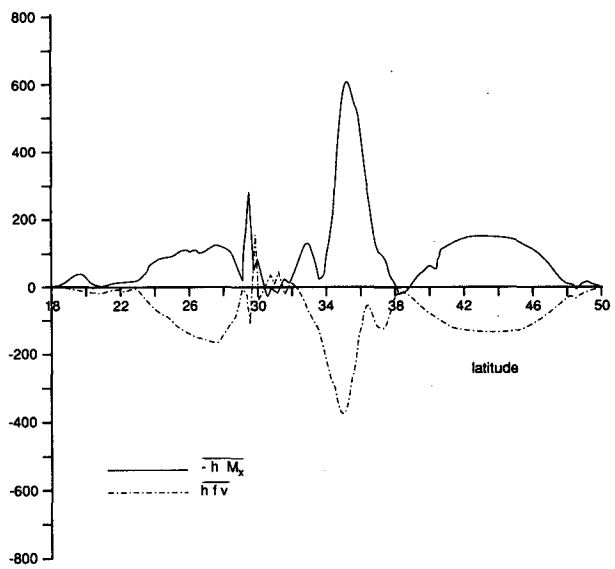

FIG. 12b. The eddy-induced change in $\overline{hfv}$ and $-\overline{hM_x}$ in the upper layer; see Fig 12a.

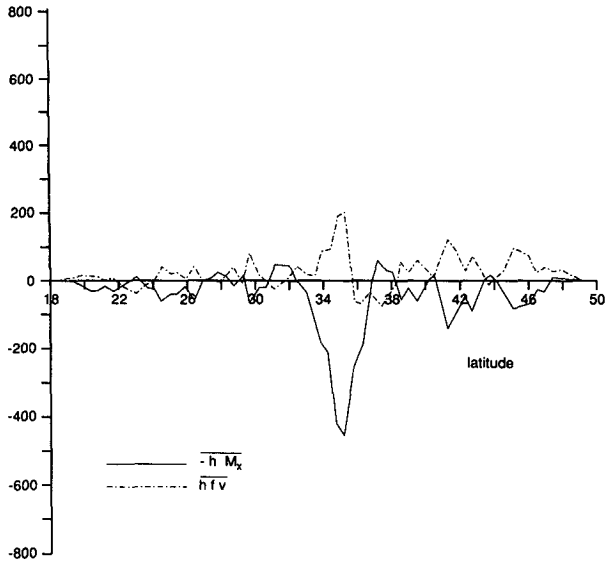

FIG. 12c. The eddy-induced change in $\overline{hfv}$ and $-\overline{hM_x}$ in the lower layers, see Fig. 12a.

where Λ is the mean flow forcing by the eddies (contrary to the atmospheric case Λ cannot simply be written as the divergence of a flux),

$$\Lambda = \{\overline{(hv)'u'}\}_y + [\overline{h'M'_x}], \tag{5.2}$$

and $\bar{X}$ is any mean nonconservative force [see appendix A for a derivation and comments on Eqs. (5.1) and (5.2)].

The effect of the transients can be elucidated by considering the balance of Eq. (5.1) for an experiment without transient eddies (experiment 1) and an experiment with transient eddies (experiment 2). Now, $[x]$ denotes the time average of x, and $\Delta[\bar{x}]$ denotes $[\bar{x}]^2 - [\bar{x}]^1$, that is, the eddy-induced change in the mean flow quantity $[\bar{x}]$. Then the change in meridional mass flux, or heat transport, can be approximated by ($\Delta\bar{X}$ is small, see appendix B)

$$\Delta[\bar{V}] = -\Delta[\Lambda - \bar{h}\bar{M}_x]/f. \tag{5.3}$$

Equation (5.3) implies that a non-heat transport behavior of the transient eddies arises whenever

$$[\Delta\Lambda] = [\bar{h}\Delta\bar{M}_x]. \tag{5.4}$$

In this equation the eddy-induced change in zonal pressure gradient is forced by the transient eddy contribution to the mean flow forcing. Figure 17 shows that this balance is approximately valid for the present model in agreement with the non-heat transport character of the eddies.

When $[\Delta\Lambda]$ and $[\bar{h}\Delta\bar{M}_x]$ are not equal to zero, Eqs. (5.3) and (5.4) imply that the eddy-induced change in the meridional mass and heat transport by the mean flow is compensated by the eddy transports themselves. The total meridional mass and heat transport remain unchanged.

The role of diabatic forcing in this balance can be elucidated by taking $\partial(5.1)/\partial y$ after time averaging and noting that $[V]_y = [Q]$, where Q is the diabatic forcing. Then Eq. (5.1) becomes

$$\partial/\partial y[\Lambda - \bar{h}\bar{M}_x + \bar{X}]/f = [\bar{Q}]. \tag{5.5}$$

Time variations in heat transport are associated with temporal mean flow changes:

$$\bar{U}_{yt} - (\Lambda - \bar{h}\bar{M}_x + \bar{X})_y = f\bar{V}_y = f(\bar{Q} - \bar{h}_t). \tag{5.6}$$

From Eq. (5.5) it is seen that $[\Lambda - \bar{h}\bar{M}_x + \bar{X}]_y$ is zero when $\bar{Q}$ is zero. Without diabatic forcing the advection of heat is immediately coupled to a change in layer thickness. But such changes are reversible: isolated eddies are ultimately captured by the mean flow without air–sea interaction altering their SST anomalies. In the time mean the eddy–mean flow interaction principle expressed by Eq. (5.4) follows from Eq. (5.6); the time-averaged total mass and heat transport remain unchanged.

When $\bar{Q}$ is small, that is, typical variations in $\bar{Q}$ smaller than typical variations in $\bar{V}_y$, the same compensation mechanism applies and Eq. (5.4) remains approximately valid.

When $\bar{Q}$ is large, however, variations in $\bar{Q}$ start dominating variations in $\bar{V}_y$ and mean flow changes

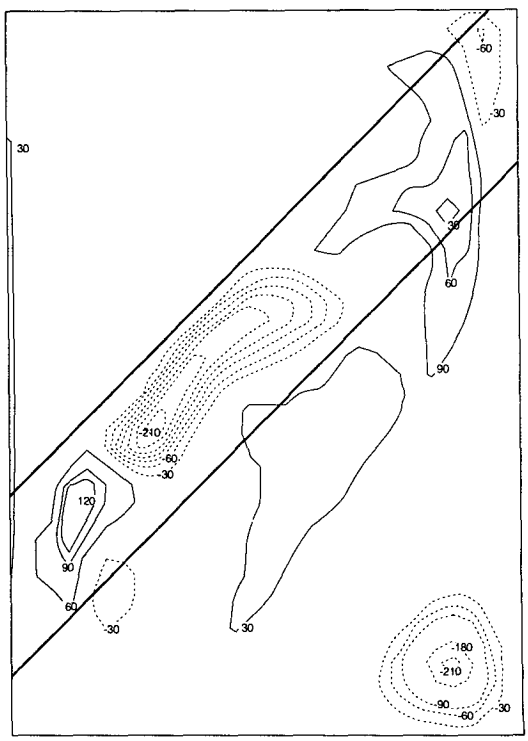

FIG. 13. The difference in upper-layer thickness between experiments 1 and 2.

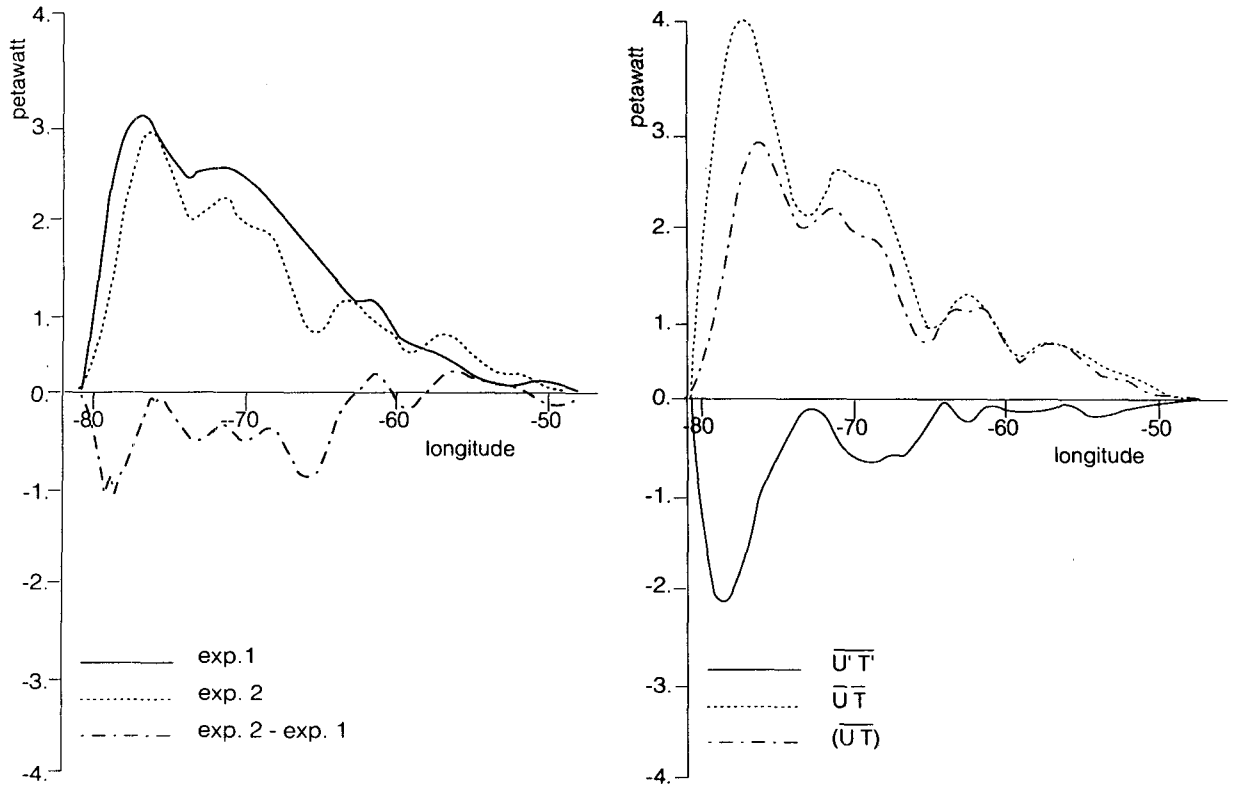

FIG. 14. (a: left) The zonal heat transport in the Gulf Stream region (see Fig. 13) as a function of longitude for experiments 1 and 2. Temperature is defined relative to the temperature of the lowest layer. (b: right) The zonal heat transport for experiment 2. Shown are the total heat transport, the eddy heat transport, and heat transport by the mean flow. The heat transport is relative to the transport in the lowest layer.

become irreversible: rings release their SST anomalies to the atmosphere before they are captured by the mean flow. In that case there is no argument why $f\Delta[\bar{Q}]$ and $f\Delta[\bar{V}]_y$ should be smaller than $\Delta[\Lambda]_y$ and $\Delta[\bar{h}\bar{M}_x]_y$, and thus no argument why Eq. (5.4) should remain valid.

The conjecture that Eq. (5.4), and consequently the non-heat transport character of the eddies, breaks down for large $\bar{Q}$ cannot be proven by the present study and is still hypothetical. A sensitivity study to the diabatic forcing $\bar{Q}$ is needed to verify or falsify this hypothesis. But, if true, we can predict from the arguments presented above for which values of $\bar{Q}$ Eq. (5.4) breaks down. Here, $[\bar{Q}]$ can be written as [see Eq. (2.4)]

$$[\bar{Q}] = (h^* - [\bar{h}])/\tau. \tag{5.7}$$

In this equation τ is the relaxation time for SST anomalies.

The diabatic forcing $\bar{Q}$ becomes important in determining the eddy–mean flow interactions when variations in $\bar{Q}$ become of the order of variations in $\bar{V}_y$. This is the case when $1/\tau$ becomes of the order of $\bar{v}/L_y$; where $\bar{v}$ is the meridional velocity of the eddies and L_y the meridional length scale.

Now $L_y = 2\pi R_d$, where R_d is the internal Rossby radius of deformation, and $v = X/(\beta L_{\text{wind}} H)$, where X is the wind stress, and H the depth of the mixed layer. For the present model the nondimensional parameter $\mu = L_y/(v\tau) = 0.3$. As μ is smaller than one, this indicates that the model is in the regime of weak diabatic forcing. The turnover point would follow from a decrease of the relaxation time τ from 333 to 100 days. Note that the model upper layer is on the average 200 m; for models with a thinner upper layer the turnover value for τ would be smaller, dependent on the depth of the actual wind-mixed layer in the model.

In summary, we may say that for weak diabatic forcing the eddy–mean flow interaction expressed by Eq. (5.4) secures the non-heat transport behavior by the eddies. For strong diabatic forcing the eddy–mean flow interaction is likely to change, and we hypothesize that Eq. (5.4) breaks down. A nondimensional parameter is provided to measure the relative strength of the diabatic forcing, which depends on the relaxation time of SST anomalies. In reality this relaxation time τ is not known exactly. Small SST anomalies will have smaller time scales than large SST anomalies, and the effective diabatic forcing for mesoscale features will be stronger than for large-scale anomalies. Also, the depth of the

mixed layer will influence the relaxation time scale, and it is likely that τ will vary with the seasonal cycle. However, we guess that for most SST anomalies τ will lie between 10 and 200 days. This would indicate that the actual atmosphere–ocean coupling is somewhere in the intermediate region, depending on the phenomena under consideration.

6. Summary and conclusions

The present numerical experiments have been designed to test whether compensation of the poleward eddy heat transport found in the numerical models of Cox (1985) and Böning and Budich (1992) also occurs within an isopycnic model, and whether it also occurs when the flow becomes so strong that the eddy heat transport can no longer be considered as a perturbation of the total heat transport but locally becomes a first-order quantity. The experiments have been carried out with an isopycnic model, derived from the code of Bleck and Boudra (1986), that simulates the idealized North Atlantic gyre study of Semtner and Mintz (1977). They consist of an intercomparison of model versions with various grid sizes, up to $1/6° \times 1/6°$ resolution, and various friction parameterizations. Results show that compensation of the eddy heat transport occurs also in this model configuration.

A second objective of this study is to provide for additional diagnostics to contribute to the discussion on the mechanism of this compensation. We assume, following Bryan (1991), that compensation of the poleward eddy heat transport consists of an increase of the wind-scale overturning cells and the associated heat transport. These cells must be interpreted as complex wind–buoyancy–eddy-driven meridional overturning cells.

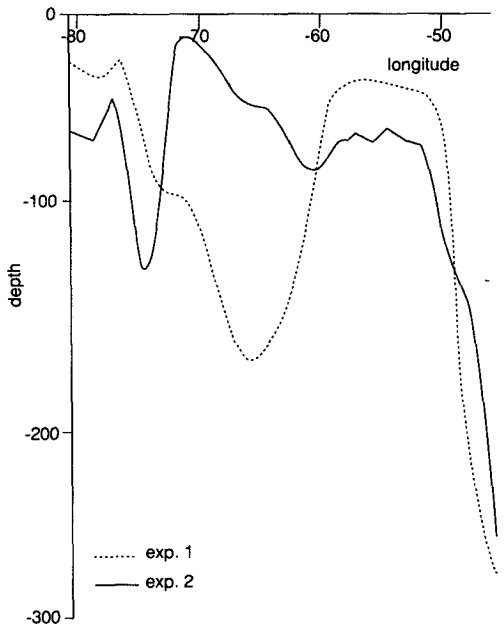

FIG. 15. The upper-layer thickness as a function of latitude, averaged over a zonal band of 4° width in the Gulf Stream region (see Fig. 13) for experiments 1 and 2.

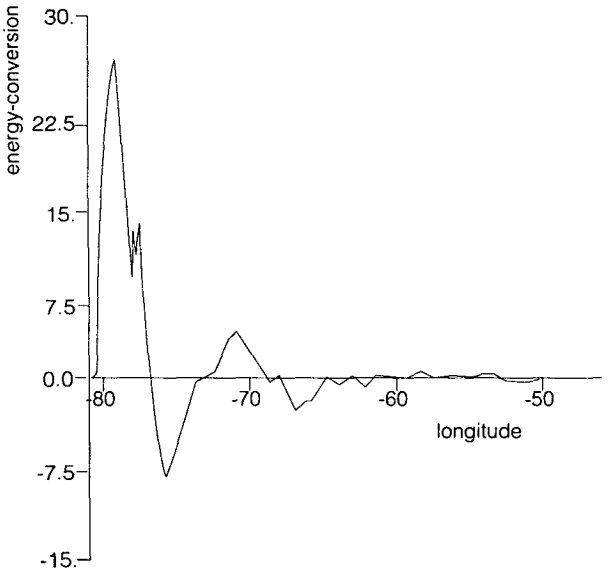

FIG. 16. The conversion from mean to eddy potential energy (in J m^{-2} s^{-1}) in the Gulf Stream region as a function of longitude.

We have confirmed Bryan's (1986) argument that the enhancement of the overturning at midlatitudes is mainly associated with a decrease of the upper-layer cross-basin zonal pressure difference there and an increase in the lower layers. The modification in cross-basin pressure difference is a baroclinic feature, associated with an eddy-induced change in the zonal heat transport at midlatitudes. This zonal eddy heat transport is against the direction of the mean flow and is strongest where the stream turns from a meridional to a zonal direction. It is associated with the baroclinic instability of the flow, which induces a downgradient eddy heat transport in both meridional and zonal directions. This reduces the mean east–west temperature gradient in the upper layer, and, as a consequence, the mean east–west pressure gradient. The subsequent increase of the meridional overturning counteracts the meridional eddy heat transport.

In the present model, the compensation occurs at midlatitudes: the largest meridional eddy heat transport is associated with the baroclinic instability of the central jet. In the simulations of Cox (1985) and Böning and Budich (1992), the largest meridional eddy heat transport is within the recirculation zone, and the overturning cell in the subtropical gyre is enhanced.

We have followed the suggestion of Bryan (1991) to discuss the compensation of the eddy heat transport using the generalized wave–zonal mean flow theory, as set out by Andrews and McIntyre (1976). This the-

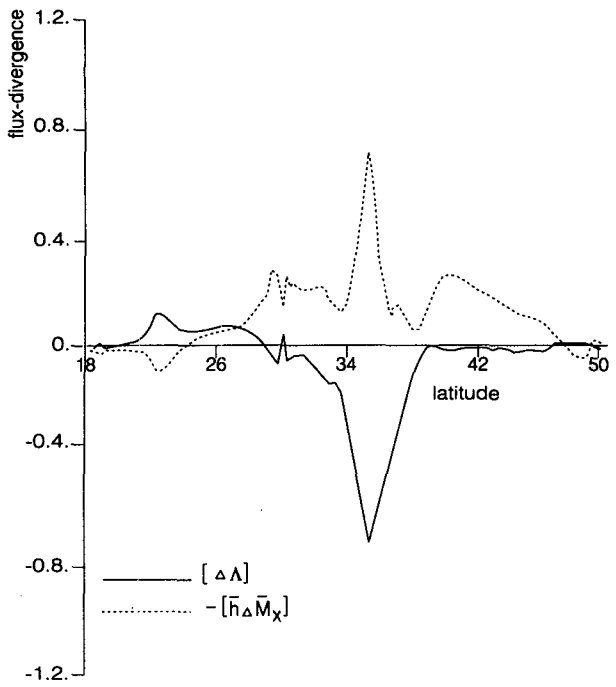

FIG. 17. The transient eddy contribution (in 10^{-2} m^2 s^{-1}) to the mean flow forcing [$\Delta\Lambda$] and the eddy-induced change in cross-basin zonal pressure difference $-[\bar{h}\Delta\bar{M}_x]$.

ory predicts a compensation for eddy transports when the eddy field is steady and conservative, and the Eliassen–Palm flux divergence is zero.

The applicability of this theory to the time-averaged ocean circulation and transient eddies is far from trivial. The assumption that the ocean eddies behave like steady waves seems inconsistent with processes like ring formation (e.g., Drijfhout 1990). Moreover, such a theory is complicated by wind and diabatic forcing and the presence of zonal barriers. In the present model the contribution of the transient eddies to the mean flow forcing is almost balanced by an eddy-induced change in zonal pressure gradient across the basin. This eddy–mean flow interaction secures the nonheat transport character of the eddies, when the eddy field is nonsteady.

The strength of the atmosphere–ocean coupling is essential in the determination of the eddy–mean flow interaction. The nonheat transport character of the eddies has only been demonstrated under weak diabatic forcing. With respect to rings this implies that diabatic effects must be small during the period that they are isolated and modification of their SST anomalies must be small. It is hypothesized that the nonheat transport character of the eddies breaks down when the diabatic forcing is sufficiently strong. A nondimensional parameter to measure the strength of the diabatic forcing suggests that this break down already might occur for realistic values of the forcing.

Acknowledgments. This research was supported by the European Economical Community (EEC). Arie Kattenberg, Theo Opsteegh, Will de Ruijter, and two anonymous reviewers are acknowledged gratefully for comments on an earlier version on this manuscript and discussion from which this study benefited.

APPENDIX A

The Zonal Mass Flux Equation

We start with the momentum equation in isopycnic coordinates:

$$u_t + uu_x + vu_y - fv + M_x = W + D_u, \quad \text{(A1)}$$

where W is the wind forcing and D_u is the friction.

The equation for layer thickness is

$$h_t + (hu)_x + (hv)_y = Q + D_h, \quad \text{(A2)}$$

where Q is the diabatic forcing and D_h is the diffusion. These two equations combine into

$$(hu)_t + (hu^2)_x + (huv)_y - fhv + hM_x = h(W + D_u) + u(Q + D_h). \quad \text{(A3)}$$

If the right-hand side is equated to X; this equation becomes, after zonal averaging,

$$(\overline{hu})_t + (\overline{huv})_y - \overline{fhv} + \overline{hM}_x = \bar{X}; \quad \text{(A4)}$$

$(\overline{huu})_x$ is zero because of the boundary conditions.

Now we write $hu = U$, $hv = V$. Also Eq. (A4) can be developed in mean and eddy terms:

$$\bar{U}_t = \bar{V}(f - \bar{u}_y) - \bar{u}\bar{V}_y - \{\overline{(hv)'u'}\}_y - \overline{h'M'}_x - \bar{h}\bar{M}_x + \bar{X}. \quad \text{(A5)}$$

The quasigeostrophic approximation for this equation consists of neglecting $\bar{u}/L_y$ compared to f, where L_y is a typical meridional length scale; see also Andrews et al. (1983). Note that $\bar{M}_x$ is not zero because of the presence of zonal barriers in the ocean. Equation (A5) then becomes

$$\bar{U}_t = f\bar{V} + \Lambda - \bar{h}\bar{M}_x + \bar{X} \quad \text{(A6)}$$

and

$$\Lambda = -\{\overline{(hv)'u'}\}_y - \overline{h'M'_x}. \quad \text{(A7)}$$

Contrary to the atmospheric case, $\overline{h'M'_x}$ is not equal to $(\overline{p'M'_x})_\rho/g$, as $\overline{pM_{x\rho}}$ is not zero because of the presence of zonal barriers; see also Andrews (1983).

APPENDIX B

The Eddy-induced Change in Forcing

We compare two experiments: one without transient eddies (experiment 1), and one with transient eddies (experiment 2). We define $\Delta x = x^1 - x^2$, where the superscript denotes the experiment. The zonal mean of x is defined as $[x]$. After zonal averaging the transient

eddy-induced change in the balance of Eq. (A6) becomes

$$\Delta[\bar{V}] = -\Delta[\Lambda - \bar{h}\bar{M}_x + \bar{X}]/f, \qquad \text{(B1)}$$

and

$$X = h(W + D_u) + u(Q + D_h) \qquad \text{(B2)}$$

[see also Eqs. (A1)–(A2)].

First, we assume that changes in friction and diffusion are small. Also, $\Delta\bar{W}$ should be zero if the equations are integrated to below the wind-mixed layer. So $\Delta[\bar{X}]/f$ is approximately equal to $\Delta[\overline{uQ}]/f$. As $\Delta[\bar{V}]$ in Eq. (B1) equals $\int \Delta[\bar{Q}]dy$, the neglect of $\Delta[\bar{X}]/f$ in Eq. (B1) is consistent with the quasigeostrophic approximation made earlier.

REFERENCES

Andrews, D. G., 1983: A finite-amplitude Eliassen–Palm theorem in isentropic coordinates. *J. Atmos. Sci.*, **40,** 1877–1883.

——, 1990: On the forcing of time-mean flows by transient, small-amplitude eddies. *J. Atmos. Sci.*, **47,** 1837–1844.

——, and M. E. McIntyre, 1976: Planetary waves in horizontal and vertical shear: The generalized Eliassen–Palm relation and the mean zonal acceleration. *J. Atmos. Sci.*, **33,** 2031–2048.

——, J. R. Holton, and C. B. Leovy, 1987: *Middle Atmospheric Dynamics.* Academic Press, 489 pp.

——, J. D. Mahlman, and R. W. Sinclair, 1983: Eliassen-Palm diagnostics of wave–mean flow interaction in the GFDL "SKYHI" general circulation model. *J. Atmos. Sci.*, **40,** 2768–2784.

Bleck, R., and D. B. Boudra, 1986: Wind driven spin-up in eddy-resolving ocean models formulated in isopycnic and isobaric coordinates. *J. Geophys. Res.*, **91,** 7611–7621.

——, and L. T. Smith, 1990: A wind-driven isopycnic coordinate model of the North and equatorial Atlantic Ocean. 1. Model development and supporting experiments. *J. Geophys. Res.*, **95,** 3273–3285.

Böning, C. W., and M. D. Cox, 1988: Particle dispersion and mixing of conservative properties in an eddy-resolving model. *J. Phys. Oceanogr.*, **18,** 320–338.

——, and R. C. Budich, 1992: Eddy dynamics in a primitive equation model: Sensitivity to horizontal resolution and friction. *J. Phys. Oceanogr.*, **22,** 361–381.

Bryan, F. O., 1987: Parameter sensitivity of primitive equation ocean general circulation models. *J. Phys. Oceanogr.*, **17,** 970–985.

Bryan, K., 1986: Poleward buoyancy transport in the ocean and mesoscale eddies. *J. Phys. Oceanogr.*, **16,** 927–933.

——, 1987: Potential vorticity in models of the ocean circulation. *Quart. J. Roy. Meteor. Soc.*, **113,** 713–734.

——, 1991: Poleward heat transport in the ocean. *Tellus,* **43,** 104–115.

Cox, M. D., 1985: An eddy-resolving numerical model of the ventilated thermocline. *J. Phys. Oceanogr.*, **15,** 1312–1324.

——, 1987: An eddy resolving numerical model of the ventilated thermocline: Time dependence. *J. Phys. Oceanogr.*, **17,** 1044–1056.

——, and K. Bryan, 1984: A numerical model of the ventilated thermocline. *J. Phys. Oceanogr.*, **14,** 674–687.

Dewar, W. K., and J. M. Bane, 1989: Gulf Stream dynamics. Part II: Eddy dynamics at 73°W. *J. Phys. Oceanogr.*, **19,** 1574–1587.

Drijfhout, S. S., 1990: Ring genesis and the related transports of heat, momentum and vorticity: A parameter study. *J. Phys. Oceanogr.*, **20,** 1645–1665.

——, 1992: Ring genesis and the related heat transport. Part II: A model comparison. *J. Phys. Oceanogr.*, **22,** 268–285.

Eliassen, A., and E. Palm, 1961: On the transfer of energy in stationary mountain waves. *Geofys. Publ.*, **22,** No. 3, 1–23.

Haney, R. L., 1971: Surface thermal boundary condition for ocean circulation models. *J. Phys. Oceanogr.*, **1,** 241–248.

Holland, W. R., 1978: The role of mesoscale eddies in the general circulation of the ocean—Numerical experiments using a wind driven quasigeostrophic model. *J. Phys. Oceanogr.*, **8,** 363–392.

——, T. Keffer, and P. B. Rhines, 1984: Dynamics of the ocean general circulation: The potential vorticity field. *Nature,* **308,** 698–705.

Hoskins, B. J., I. N. James, and G. N. White, 1983: The shape, propagation and mean-flow interaction of large-scale weather systems. *J. Atmos. Sci.*, **40,** 1595–1612.

Huang, R. X., 1989: Sensitivity of a multilayered oceanic general circulation model to the sea surface thermal boundary condition. *J. Geophys. Res.*, **94,** 18 011–18 021.

Palmen, E., and C. W. Newton, 1969: *Atmospheric Circulation Systems.* Academic Press, 603 pp.

Plumb, R. A., 1986: Three-dimensional propagation of transient quasi-geostrophic eddies and its relationship with the eddy forcing of the time-mean flow. *J. Atmos. Sci.*, **43,** 1657–1678.

Rhines, P. B., and W. Young, 1982: A theory of the wind-driven ocean circulation. I. Mid-ocean gyres. *J. Mar. Res.*, **40**(Suppl.), 559–596.

Robinson, A. R., 1983: *Eddies in Marine Science.* Springer-Verlag, 609 pp.

Semtner, A. J., and Y. Mintz, 1977: Numerical simulation of the Gulf Stream and mid-ocean eddies. *J. Phys. Oceanogr.*, **7,** 208–230.

——, and W. R. Holland, 1978: Intercomparison of quasi-geostrophic simulations of the western North Atlantic circulation with primitive equation results. *J. Phys. Oceanogr.*, **8,** 735–754.